Inhibition of Cluster Phenomena in Truly Water Soluble Fullerene Derivatives: Bimolecular Electron and Energy Transfer Processes

Dirk M. Guldi,* Hartmut Hungerbühler, and Klaus-Dieter Asmus

Radiation Laboratory, University of Notre Dame, Notre Dame, Indiana 46556

A series of water-soluble fullerene derivatives, namely, e-$C_{60}[C(COO^-)_2]_2$ (**2**), $trans$-3-$C_{60}[C(COO^-)_2]_2$ (**3**), $trans$-2-$C_{60}[C(COO^-)_2]_2$ (**4**), and e,e,e-$C_{60}[C(COO^-)_2]_3$ (**5**) were probed in light- and radical-induced studies and compared to $\{(^3C_{60})C(COO^-)_2\}_n$ clusters (**1**). Ground-state absorption spectra of **2**–**5**, recorded in a concentration range between 1.0×10^{-4} M and 5×10^{-6} M, clearly speak against any appreciable deviation from the Lambert–Beer law. Picosecond-resolved photolysis gives rise to singlet excited state absorptions that closely resemble earlier observations for e-$C_{60}[C(COOEt)_2]_2$, $trans$-3-$C_{60}[C(COOEt)_2]_2$, $trans$-2-C_{60}-$[C(COOEt)_2]_2$, and e,e,e-$C_{60}[C(COOEt)_2]_3$ in deoxygenated toluene solutions. The triplet lifetimes of **2**–**5**, as measured by nanosecond-resolved photolysis, are typically around 40 μs, similar to the triplet lifetimes of truly monomeric fullerene solutions. A strongly enhanced lifetime (by nearly 3 orders of magnitude) relative to $\{(^3C_{60})C(COO^-)_2\}_n$ clusters (**1**) ($\tau = 0.4$ μs) indicates a truly monomeric appearance of these bis- and tris-functionalized fullerenes in aqueous solutions and confirms that micellar aggregation does, indeed, play only a minor role regarding the reactivity of these derivatives. Quenching experiments with diazabicyclooctane (DABCO), involving the triplet excited states of **2**–**5**, yielded rate constants which reveal a strong dependence on the degree of functionalization. They vary between 7.4×10^7 M^{-1} s^{-1} and 5.1×10^5 M^{-1} s^{-1}. This clearly indicates a substantial shift in the redox potential of the triplet excited state between pristine C_{60} and e,e,e-$C_{60}[C(COO^-)_2]_3$ (**5**). As a consequence of reductive quenching, the spectral region between 900 and 1100 nm shows the time-resolved growths of the π-radical anion absorptions with maxima at 1040, 995, 880, and 1020 nm, for **2**, **3**, **4**, and **5**, respectively. They match the spectra generated by means of hydrated electrons ($k = (0.75-3.4) \times 10^9$ M^{-1} s^{-1}) and $(CH_3)_2$•COH radicals ($k = (0.9-2.2) \times 10^8$ M^{-1} s^{-1}) in pulse radiolysis experiments.
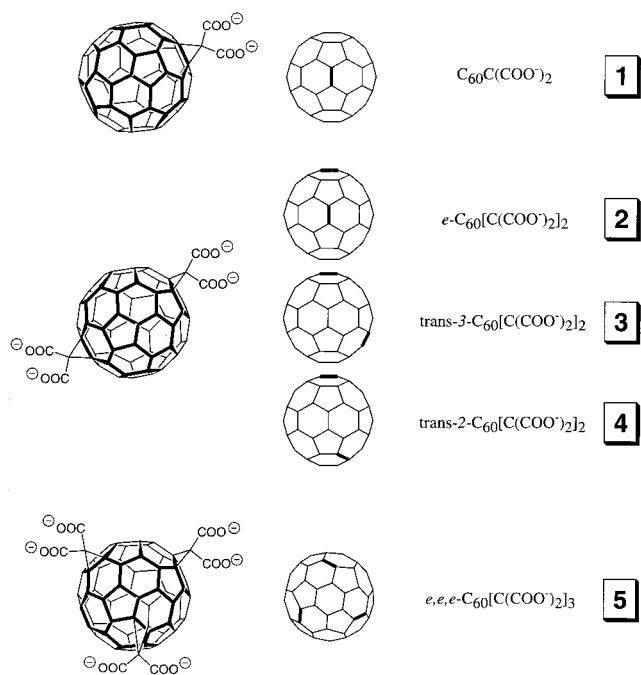
Introduction

The unique symmetry of C_{60} and its higher analogues evoked a lively and interdisciplinary interest to probe them as three-dimensional π-systems and to relate their properties to conventional two-dimensional π-sytems. In fact, the three-dimensional structure leads to a substantial curvature of the carbon network and, in turn, to a strong pyramidalization of the individual carbon atoms with an average σ-bond hybridization of sp$^{2.278}$ and a fractional s-character of the p-orbitals of 0.085.[1] The sum of these effects has a strong impact on the reactivity of the fullerene core, leading in essence, to a very reactive exterior surface but nearly inert interior part.[2] In addition, the electronic configuration of fullerenes, comprising a 5-fold degenerate HOMO (h_u) and a triply degenerate LUMO (t_{1u}), is characterized by a small energy gap (ca. 1.8 eV).[3,4] A direct consequence, which derives from this energy gap, leads to the application of C_{60} and functionalized derivatives as electron acceptor moieties. This aspect was further substantiated by means of electrochemical measurements.[5-7] Moreover, an exceptionally low reorganization energy of the fullerene core is directly associated with a high degree of charge and energy delocalization within the carbon framework.[8,9] Accordingly, forward electron transfer and charge separation are strongly favored, while, at the same time, back electron transfer experiences a noticeable slowdown relative to conventionally used electron acceptors, such as two-dimensional aromatic molecules, methyl viologen, quinones, etc.[10]

For bimolecular electron transfer dynamics and stabilization of charge-separated radical pairs, solvents of high polarity, including aqueous solutions, serve a key function in retarding undesired, fast back electron transfer. There are also tremendous biological implications that have been triggered by the advent of fullerenes. They range from potential inhibition of HIV-1 protease and synthesis of drugs for photodynamic therapy to participation in photoinduced DNA scission processes.[11] These examples unequivocally demonstrate the particular importance of water-soluble fullerenes.

With this objective in mind, numerous synthetic routes have been developed to overcome the hydrophobicity of the fullerene framework.[12-15] Cyclopropylation with bromomalonic acid diethyl ester is a versatile and, furthermore, an easily handable approach for the controlled functionalization of the fullerene core.[16] Stepwise addition of malonic acid diethyl ester leads, in case of C_{60}, in the first instance to the formation of a single monoadduct $C_{60}C(COOEt)_2$ and, upon exhaustive reaction, to defined regioisomeric bis and tris adducts, $C_{60}[C(COOEt)_2]_n$ ($n = 2, 3$).[17] The desired water soluble carboxylic acid derivatives, $C_{60}[C(COO^-)_2]_n$ ($n = 2, 3$), are readily obtained via hydrogenolosis of these ester precursors.[18]

Functionalization of C_{60}, by means of one or more consecutive addition reactions, yields a new material with appealing and technologically promising characteristics.[14] Most importantly, the extended and highly delocalized π-system experiences a gradual destruction.[19,20] Specifically, a perturbation is noticed which depends strongly on (i) the degree of functionalization,

* Corresponding author. E-mail: guldi.1@nd.edu.

Bimolecular Electron and Energy Transfer Processes

J. Phys. Chem. B, Vol. 103, No. 9, 1999 **1445**

Figure 1. Compunds used in this study.

(ii) the relative distance of the individual addends to each other, and (iii) the electronic structure of the substituent.

Recently, we reported on the radical-induced reduction of a series of water-soluble monoadducts bearing either charged headgroups, e.g., carboxylic or pyrrolidinium functionalities, or nonionic addends.[21−23] Fullerenes, i.e., C_{60}, C_{70}, C_{76}, C_{78}, and C_{84}, and various monofunctionalized fullerene derivatives have been found to be good electron acceptor moieties that are readily reduced by suitable agents, such as solvated electrons and α-hydroxy alkyl radicals.[24] No such reaction was, however, observed in an attempt to verify a radical-induced reduction of, for example, $C_{60}C(COO^-)_2$. This, at first glance, surprising inertness has been ascribed to an instaneous fullerene aggregation which takes place in aqueous solution, a conclusion that is further based on the fact that the singlet ground-state spectrum is overshadowed by strong light scattering. Accordingly, a micellar aggregation has been suggested with the hydrophobic fullerene core in the center shielded by the hydrophilic carboxyl groups pointing toward the aqueous phase from the electron attack.

Introduction of a second and, subsequently, a third hydrophilic ligand to the C_{60} core leads to three-dimensional architectures, which, in essence, display an enhanced surface coverage of the hydrophobic fullerene surface. As a consequence, fullerene aggregation may be impacted to a noticeable extent due to intermolecular π−π association. The present study will demonstrate, by means of probing a series of $C_{60}[C(COO^-)_2]_2$ and e,e,e-$C_{60}[C(COO^-)_2]_3$ in light- and radical-induced studies, that micellar aggregation does, indeed, play only a minor role in the reactivity of these functionalized fullerenes.

Experimental Section

C_{60} was purchased from Hoechst AG and diazabicylooctane (DABCO) from Aldrich. The e-$C_{60}[C(COOEt)_2]_2$, *trans-3*-C_{60}-$[C(COOEt)_2]_2$, *trans-2*-$C_{60}[C(COOEt)_2]_2$, and e,e,e-$C_{60}[C(COOEt)_2]_3$ were synthesized according to a method described already.[17,18] Hydrolysis of these ester derivatives, affording the e-$C_{60}[C(COO^-)_2]_2$ (**2**), *trans-3*-$C_{60}[C(COO^-)_2]_2$ (**3**), *trans-2*-C_{60}-$[C(COO^-)_2]_2$ (**4**), and e,e,e-$C_{60}[C(COO^-)_2]_3$ (**5**) (see Figure 1),

respectively, was carried out following two different procedures on which we reported earlier.[22]

Pulse radiolysis experiments were performed by utilizing either 500 ns pulses of 1.55 MeV electrons from a Van de Graaff accelerator facility or 50 ns pulses of 15 MeV electrons from a linear electron accelerator (LINAC). Essential details of the equipment and the data acquisition have been described elsewhere.[25] Dosimetry was based on the oxidation of SCN^- to $(SCN)_2^{•-}$ which in aqueous, N_2O-saturated solution takes place with $G \approx 6$ (G denotes the number of species per 100 eV, or the approximate micromolar concentration per 10 J absorbed energy). The radical concentration generated per pulse was varied between $(1-3) \times 10^{-6}$ M for all the systems investigated in this study.

For flash photolysis studies, the fullerene concentrations were prepared to exhibit an optical density of at least 0.2 at 337 nm, the wavelength of irradiation. The apparatus for laser-flash photolysis has been described earlier.[26,27] Nanosecond laser flash photolysis experiments were performed with laser pulses from a Molectron UV-400 nitrogen laser system (337.1 nm, 8 ns pulse width, 1 mJ/pulse) in a front face excitation geometry. A Xe lamp was triggered synchronously with the laser. A monochromator (SPEX) in combination with either a Hamamatsu R 5108 photomultiplier or a fast InGaAs diode was employed to monitor transient absorption spectra.

Cyclic voltametry measurements were performed with a glassy carbon rotating working electrode, polished with a 1 μm diamond paste before each run, a Pt counter electrode, and an aqueous standard calomel electrode as reference. The electrochemical set up has been described in detail elsewhere.[19]

All radiolytic investigations were conducted in nitrogen-saturated, dilute aqueous solutions containing 10 vol % 2-propanol. This condition leads to the production of three highly reactive species, namely $^•H$, $^•OH$, and e_{aq}^-, beside the molecular products H^+_{aq}, H_2, and H_2O_2.

$$H_2O \xrightarrow{radiolysis} {}^•H, {}^•OH, e_{aq}{}^-, H^+{}_{aq}, H_2, H_2O_2 \qquad (1)$$
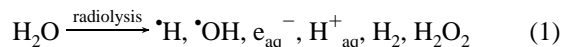
2-Propanol efficiently scavenges two of the radical species, namely $^•OH$ and $^•H$ radicals, via hydrogen abstraction (eq 2).

$$(CH_3)_2CHOH + {}^•OH\ ({}^•H) \rightarrow (CH_3)_2{}^•COH + H_2O\ (H_2) \quad (2)$$
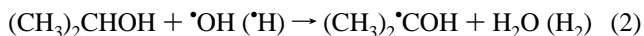
The main resulting radical, $(CH_3)_2{}^•COH$, is a powerful reductant that has been shown to rapidly reduce, for example, pristine C_{60}. For the determination of the individual rate constants, e.g., for the reduction of fullerenes by hydrated electrons or $(CH_3)_2{}^•C(OH)$ radicals, the following experimental condition were chosen.

Hydrated Electrons (e_{aq}^-). Substitution of 2-propanol by *tert*-butanol, which converts $^•OH$ radicals into the reduction-inert $^•CH_2(CH_3)_2COH$ species. This, in turn, leaves the hydrated electron as the only reactive entity.

$$CH_3(CH_3)_2COH + {}^•OH\ ({}^•H) \rightarrow$$
$${}^•CH_3(CH_3)_2COH + H_2O\ (H_2) \quad (3)$$
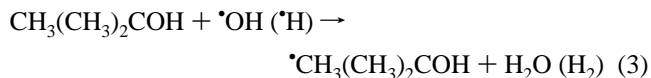
$(CH_3)_2{}^•C(OH)$ Radicals. Deaeration of the aqueous 2-propanol solution with N_2O rather than N_2. This results in the quantitative scavenging of hydrated electrons and conversion of the latter into hydroxyl radicals.

$$N_2O + e_{aq}{}^- + H_2O \rightarrow N_2 + {}^•OH + {}^-OH \qquad (4)$$
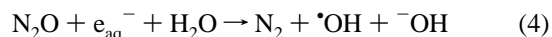
Results and Discussion

Ground-State Properties. *Absorption Spectra.* The water-soluble monoadduct $C_{60}C(COO^-)_2$ (**1**) has been found to display
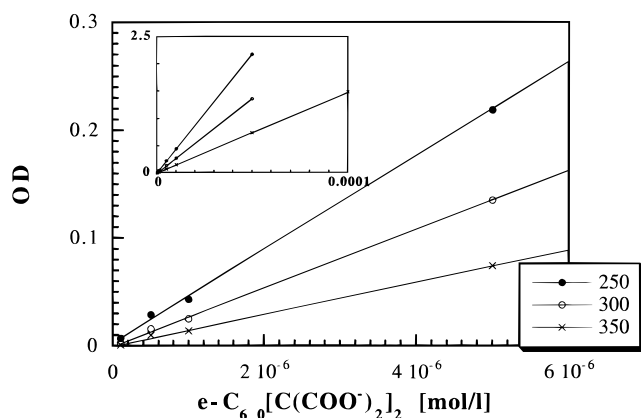
Figure 2. Plot of the absorbance at 250 (●), 300 (○), and 350 nm (×) versus the concentration of e-$C_{60}[C(COO^-)_2]_2$ (**2**) in aqueous solution at room temperature. Inset shows the dependence over the entire concentration range, i.e., 1.1×10^{-6} to 1.0×10^{-4} M.

substantial association in aqueous solution.[22] Following the concept of decreasing the hydrophobic fullerene surface, it may be expected that e-$C_{60}[C(COO^-)_2]_2$ (**2**) shows a slightly different aggregation behavior in aqueous solution. Hence, it seemed appropriate to ask whether the singlet ground-state spectrum of compounds **2**−**5** reveals any noticeable deviation from the Lambert−Beer law. Typical spectroscopic measurements, with respect to the singlet ground-state absorptions of e-C_{60}-$[C(COO^-)_2]_2$ (**2**), were carried out at various wavelength, i.e., 250, 300, and 350 nm, and are summarized in Figure 2. A wide range of substrate concentrations, e.g., between 1.0×10^{-4} and 5×10^{-6} M, were utilized for these studies which, furthermore, represent typical fullerene concentrations used for the envisaged time-resolved pulse radiolytic and flash photolytic investigations. The linear correlation that can be derived, for example, for derivative **2** at all plotted wavelengths over the applied fullerene concentration clearly speaks against any appreciable deviation from the Lambert−Beer law.

Complementary spectroscopic measurements were also carried out with *trans-3*-$C_{60}[C(COO^-)_2]_2$ (**3**), *trans-2*-$C_{60}[C(COO^-)_2]_2$ (**4**), and e,e,e-$C_{60}[C(COO^-)_2]_3$ (**5**) in a similar concentration window. In line with the observation described for e-C_{60}-$[C(COO^-)_2]_2$ (**2**), the linear dependencies are again interpreted as a successful suppression of the strong aggregation forces noticed for pristine C_{60} and some water-soluble monofunctionalized fullerene derivatives in aqueous media.

Excited-State Properties. *Fluorescence Spectra as a Sensitive Probe for Clustering.* The singlet excited states of fullerenes, C_{60}, etc., are efficiently populated via irradiation into their extensive absorption bands throughout the UV and visible region. Due to a nearly quantitative intersystem crossing process between the singlet excited state and triplet excited state, the fluorescence quantum yields of functionalized fullerene derivatives are generally very low, ranging between 2.0×10^{-4} and 6.0×10^{-4}.[28] Nevertheless, the spectral convolution of the *0 → 0 band, representing the radiative transition from a vibrational state (ν = 1, 2, 3, 4, etc.) of the singlet excited state to the singlet ground state (eq 5), and its relative positioning may be employed as a sensitive diagnostic tool for aggregation and other environment effects, such as hydrophilicity or hydrophobicity of the solvent or even a supermolecular host molecule.

$$e\text{-}C_{60}[C(COO^-)_2]_2 \xrightarrow{h\nu} e\text{-}(^1C_{60})[C(COO^-)_2]_2 + h\nu' \quad (5)$$
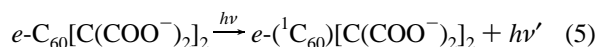
Specifically, possible cluster solutions of $\{C_{60}C(COO^-)_2\}_n$ will be compared with those of (i) the truly monomeric $C_{60}C$-
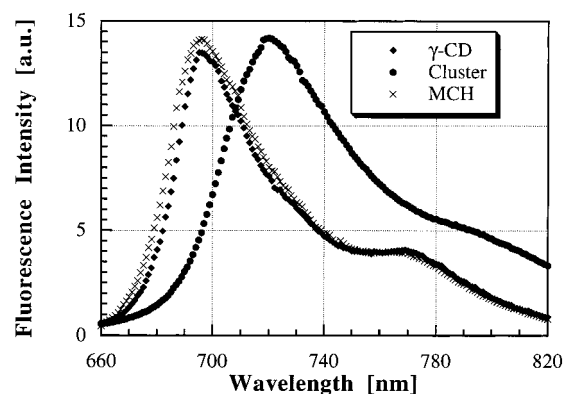
Figure 3. Fluorescence spectra of $C_{60}C(COOEt)_2$ in methylcyclohexane (×), $C_{60}C(COO^-)_2$ (**1**) cluster in homogeneous aqueous solutions (●), and $C_{60}C(COO^-)_2$ (**1**) monomers in heterogeneous aqueous solutions (γ-CD encapsulated complex) (♦) at room temperature. The fluorescence intensity is arbitrary and normalized to a comparable height.
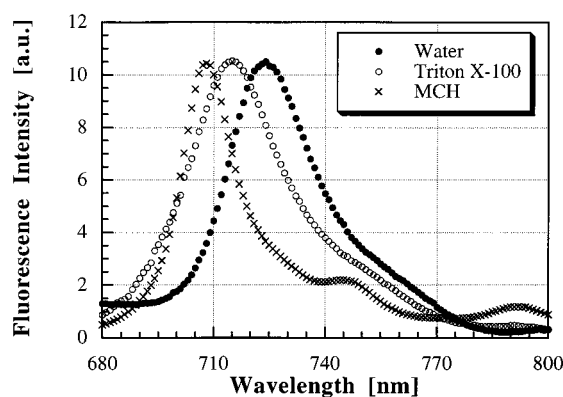
Figure 4. Fluorescence spectra of *trans-2*-$C_{60}[C(COOEt)_2]_2$ in methylcyclohexane (×), *trans-2*-$C_{60}[C(COO^-)_2]_2$ in homogeneous aqueous solutions (●), and *trans-2*-$C_{60}[C(COO^-)_2]_2$ in heterogeneous aqueous solutions (5% Triton X-100) (○) at room temperature. The fluorescence intensity is arbitrary and normalized to the same height.

$(COO^-)_2/\gamma$-CD (**1**) complex in water and (ii) the analogous ester derivative, $C_{60}C(COOEt)_2$, in methylcyclohexane. The most important feature of the fluorescence spectra (see Figure 3) is a broadening of the main emission band by going from a monomer to a cluster solution. This is accompanied by a substantial, solvent-related red shift. In line with the broadening of the singlet ground-state absorption features, this effect arises unmistakably from fullerene aggregation. Further support for this assumption is taken from the emission spectrum of a monomeric surfactant solution of **1** (not shown), which, in line with expectation, lacks such a spectral broadening.

It is worth mentioning that the emission spectrum of the γ-CD inclusion complex is nearly superimposable to that of $C_{60}C$-$(COOEt)_2$ in nonaqueous methycyclohexane. This agreement corroborates the similarity of the γ-CD interior as a microscopic solvent environment with that of nonpolar methylcyclohexane.

Measurements with, for example, *trans-2*-$C_{60}[C(COO^-)_2]_2$ (**4**) reveal overall resembling trends. Parallel to a solvent-induced red shift, e.g., in methylcyclohexane solutions (708 nm), Triton X-100 (714 nm), and aqueous solutions (723 nm), the fluorescence spectra uniformly show a fairly narrow emission band (Figure 4). The corresponding half-widths, with values of 20, 28, and 20 nm, respectively, clearly contrast those broader features described above for the cluster solution of **1**, which exhibits a half-width of 42 nm. Analogously broadened bands of the *trans-3*-$C_{60}[C(COO^-)_2]_2$ (**3**) singlet excited states assist to further confirm this trend.

Bimolecular Electron and Energy Transfer Processes

J. Phys. Chem. B, Vol. 103, No. 9, 1999 **1447**

TABLE 1: Photophysical and Spectroscopic Data for the Excitation of Functionalized Fullerene Derivatives 1−5 and Pristine C_{60} in Aqueous Solutions
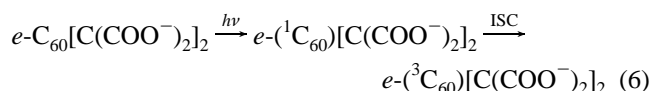
compound	$^*S_1 \rightarrow {}^*S_N$ [nm]	ISC [s^{-1}]	$^*T_1 \rightarrow {}^*T_N$ [nm]	triplet decay [s^{-1}]	$k_{quenching}$ DABCO [M^{-1} s^{-1}]	$k_{quenching}$ O_2 [M^{-1} s^{-1}]	$E_{1/2}$ [V] vs SCE
$C_{60}{}^a$			750		7.4×10^7 ^{b}	4.9×10^8 ^{b}	-0.56^b
$C_{60}C(COO^-)_2$; (**1**)^a	890	5.8×10^8	720	1.0×10^4	4.8×10^6 ^{b}	4.2×10^8 ^{b}	-0.64^c
e-$C_{60}[C(COO^-)_2]_2$; (**2**)	880	4.2×10^8	690	1.7×10^4	7.2×10^5	1.73×10^9	-0.76^c
trans-3-$C_{60}[C(COO^-)_2]_2$; (**3**)	900	5.1×10^8	670	1.4×10^4	5.1×10^5	1.51×10^9	-0.80^c
trans-2-$C_{60}[C(COO^-)_2]_2$; (**4**)	890	3.6×10^8	670	1.7×10^4	8.3×10^5	1.46×10^9	-0.76^c
e,e,e-$C_{60}[C(COO^-)_2]_3$; (**5**)			650	1.2×10^4	$< 1.0 \times 10^5$		-0.86^c

^{a} Surfactant solutions (5% Triton X-100). ^{b} γ-CD complexes. ^{c} Ester derivatives in 1,2-DCE.

In contrast, the spectra of *e*-$C_{60}[C(COO^-)_2]_2$ (**2**) are poorly resolved and show only a weak fluorescence which prevents an unambiguous analogous assignment. This observation can be rationalized, at least in part, by the similarity of the corresponding HOMO's and LUMO's of **2** as compared to pristine C_{60}, and this will be subject to further discussions (see below).

Picosecond-Resolved Photolysis. Pico- and nanosecond-resolved photolysis are important spectroscopic techniques for the characterization of dynamic processes and, accordingly, will complement the above steady-state emission studies. Specifically, they help to identify reactions that are directly and indirectly associated with the generation and fate of photoexcited states.

To probe the singlet and triplet excited state characteristics of water soluble *e*-$C_{60}[C(COO^-)_2]_2$ (**2**), *trans-3*-$C_{60}[C(COO^-)_2]_2$ (**3**), *trans-2*-$C_{60}[C(COO^-)_2]_2$ (**4**), and *e,e,e*-$C_{60}[C(COO^-)_2]_3$ (**5**), time-resolved differential absorption spectra were recorded following a 18 ps laser excitation. Transient absorption spectra of compounds **2**−**5** (2.0×10^{-5} M) in deoxygenated aqueous solutions reveal the evolution of absorptions around 900 nm (see Table 1) which are typically completed 100 ps after the laser pulse. For assignment, it is important to note that the monitored maxima closely resemble earlier observations for *e*-$C_{60}[C(COOEt)_2]_2$, *trans-3*-$C_{60}[C(COOEt)_2]_2$, *trans-2*-C_{60}-$[C(COOEt)_2]_2$, and *e,e,e*-$C_{60}[C(COOEt)_2]_3$ in deoxygenated toluene solutions.[20] On the basis of this, we attribute the transient absorptions to the fullerene singlet−singlet ($^*S_1 \rightarrow {}^*S_N$) transition, i.e., between states of identical spin. The $^*S_1 \rightarrow {}^*S_N$ decay followed clear first-order kinetics. Simultaneously, the formation of sharp absorptions, located between 650 and 750 nm were noticed, assignable to transitions from the energetically lower lying triplet excited states, namely, $^*T_1 \rightarrow {}^*T_N$. The decay kinetics of the singlet excited states (around 900 nm) and grow-in kinetics of the triplet excited states (around 700 nm) are identical and enable determination of the associated intersystem crossing rates between the two different spin states. They were consistently in the range of 5.0×10^8 s^{-1} (Table 1) and display, upon comparison with monomeric solutions of functionalized fullerene derivatives in aqueous and also nonaqueous environments, an excellent agreement with the latter.

$$e\text{-}C_{60}[C(COO^-)_2]_2 \xrightarrow{h\nu} e\text{-}(^1C_{60})[C(COO^-)_2]_2 \xrightarrow{ISC}$$
$$e\text{-}(^3C_{60})[C(COO^-)_2]_2 \quad (6)$$

Nanosecond-Resolved Photolysis. In addition, nanosecond flash photolytic experiments were conducted, using the same solute concentration as in the above picosecond studies (2.0×10^{-5} M), to complement the differential absorption changes evolving from the formation of the excited triplet state and, furthermore, to monitor the triplet decay kinetics. The lifetime of the latter is, however, an extremely sensitive probe for the aggregation status of the respective fullerene in solution. The
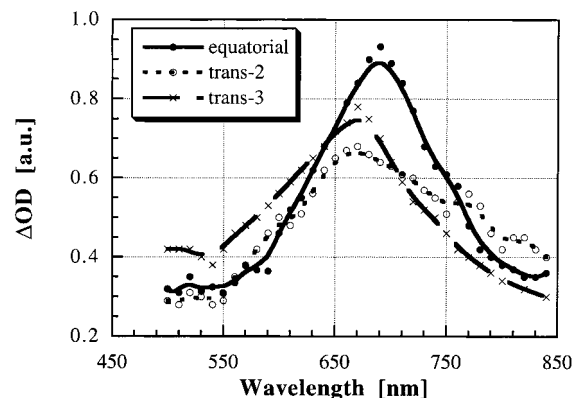
Figure 5. Differential absorption spectrum obtained upon flash photolysis at 337 nm of 2.0×10^{-5} M *e*-$C_{60}[C(COO^-)_2]_2$ (**2**) (●), *trans-3*-$C_{60}[C(COO^-)_2]_2$ (**3**) (×), and *trans-2*-$C_{60}[C(COO^-)_2]_2$ (**4**) (○) in nitrogen saturated aqueous solution.

transient absorption spectra recorded 200 ns after the laser excitation of *e*-$C_{60}[C(COO^-)_2]_2$ (**2**), *trans-3*-$C_{60}[C(COO^-)_2]_2$ (**3**), and *trans-2*-$C_{60}[C(COO^-)_2]_2$ (**4**), at 337 nm are displayed in Figure 5, exhibiting maxima at 690 (**2**) and 670 nm (**3** and **4**). Accordingly, these differential changes confirm the similarity of the transient products with those developing through the picosecond time regime in the monitored wavelength range. More importantly, it is safe to conclude that in the time window which lapses between the two time regimes, i.e., 5000 ps (picosecond) and 10 ns (nanosecond), no additional chemical or physical changes occur once photoexcitation has taken place.

Although the absorption maximum of *e*-$(^3C_{60})[C(COO^-)_2]_2$ (690 nm) is blue shifted by nearly 20 nm relative to the triplet excited state of the analogous ester derivative in toluene (710 nm) *e*-$(^3C_{60})[C(COOEt)_2]_2$,[20] the transient can, nevertheless, be ascribed to the triplet excited state *e*-$(^3C_{60})[C(COO^-)_2]_2$. A possible interaction with the aqueous environment may serve as a rationale for the observed blue shift. The half-life of 40 μs derived from the decay kinetics at $\lambda_{max} = 690$ nm and various other wavelengths is similar to the triplet lifetimes of truly monomeric fullerene solutions, such as the mono adduct (**1**) and pristine C_{60}, either encapsulated by γ-CD or incorporated into Triton X-100, e.g., $(^3C_{60})C(COO^-)_2/\gamma$-CD and $(^3C_{60})/\gamma$-CD.[23] In fact, the strongly prolonged lifetime of nearly 3 orders of magnitude relative to $\{(^3C_{60})C(COO^-)_2\}_n$ clusters ($\tau = 0.4$ μs) implies a truly monomeric appearance of this fullerene derivative (**2**) in aqueous solutions.

It is a well-established fact that the all-equatorial *e,e,e*-C_{60}-$[C(COOEt)_2]_3$ (**5**) displays the most extreme perturbation of the fullerene π-system relative to pristine C_{60}. Extrapolating the above results on the excited-state properties of *e*-$C_{60}[C(COO^-)_2]_2$ (**2**), this tris derivative should show the least detectable aggregation. In principle, this assumption has already been substantiated through the spectroscopic ground-state properties. Thus, excitation of (**5**) was also carried out in nitrogen-saturated aqueous solution without incorporation into a water soluble

superstructure. Differential absorption changes, recorded throughout the UV−vis region, gave rise to the generation of a long-lived transient species with a half-life of nearly 40 μs. The triplet excited-state absorption (*T_1→ *T_N), maximizing at 720 nm, has, however, a surprisingly strong red shift compared to *e,e,e*-($^3C_{60}$)[C(COOEt)$_2$]$_3$ (650 nm) in toluene.[20] This red shift contradicts the spectroscopic trends observed for the equatorial bis adduct (**2**) but substantiates the red-shifted absorption maximum of *e,e,e*-($C_{60}^{\bullet-}$)[C(COO$^-$)$_2$]$_3$ (1020 nm) relative to *e,e,e*-($C_{60}^{\bullet-}$)[C(COOEt)$_2$]$_3$ (1015 nm). At the moment, we cannot offer a satisfying rationale for the reversed spectral shift.

In conclusion, the steady-state and time-resolved photolytic measurements provide spectral and kinetic information on the fullerene singlet and triplet excited states with lifetimes that strongly suggest the absence of fullerene aggregates in case of the investigated bis and tris adducts.

Triplet Quenching by Oxygen. Another remarkable property of fullerenes is their key function in the generation of singlet oxygen $^1O_2(^1\Delta)$, namely, via bimolecular energy transfer between triplet excited fullerenes and molecular oxygen.[29,30] The reactivity of the triplet excited states of the water-soluble fullerene derivatives with molecular oxygen were probed by monitoring the fate of the (*T_1→ *T_N) absorption as a function of oxygen concentration. In general, addition of $(0-1.3) \times 10^{-3}$ M oxygen to the fullerene-containing samples resulted in an accelerated decay of the corresponding triplet excited-state absorption at 690 nm. In all cases, the quenching of the excited states followed eq 7, where k_{obs} refers to the observed first-order decay rate constant of the triplet excited state, k_d is the rate constant without addition of any oxygen, k_q is the bimolecular quenching rate constant, and $[Q]$ is the quencher concentration (oxygen).

$$k_{obs} = k_d + k_q[Q] \qquad (7)$$

The observed rates ($k_{obs} = \ln 2/\tau_{1/2}$) were linearly dependent on the oxygen concentration (not shown), indicating that the underlying process can be attributed to the following quenching reaction:

$$e\text{-}(^3C_{60})[C(COO^-)_2]_2 + O_2 \rightarrow e\text{-}C_{60}[C(COO^-)_2]_2 + {}^1O_2(^1\Delta) \qquad (8)$$
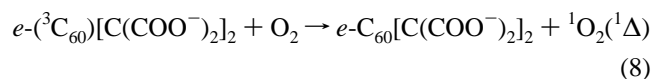
It is interesting to note that the determined values (see Table 1) imply some activation energy and even the highest rate constant of 1.73×10^9 M^{-1} s^{-1} for $k_{quenching}$ of *e*-($^3C_{60}$)-[C(COO$^-$)$_2$]$_2$ is still lower than the diffusion limit (6.5×10^9 M^{-1} s^{-1}).[31]

Photoinduced Electron Transfer from a Sacrificial Electron Donor. As a direct consequence of populating an excited state, reduction and oxidation steps are energetically enhanced by precisely the excited-state energy. Thus, the excited-state properties of the current water-soluble fullerene derivatives were probed with regard to electron transfer processes with a sacrificial electron donor. On a previous occasion, we had reported that the quenching kinetics, performed with a variety of fullerene derivatives, changed dramatically with increasing degree of functionalization.[19] The relationship found followed closely the electron accepting properties of the singlet ground-state fullerene complexes.

Addition of a suitable quencher, such as diazabicyclooctane (DABCO), to the aqueous *e*-C$_{60}$[C(COO$^-$)$_2$]$_2$ (**2**) (pH 9.7) solution results in an accelerated decay of the *T_1→ *T_N absorption at 690 nm. Kinetic measurements in the range of 0.05−0.2 M DABCO disclosed a linear dependence of the
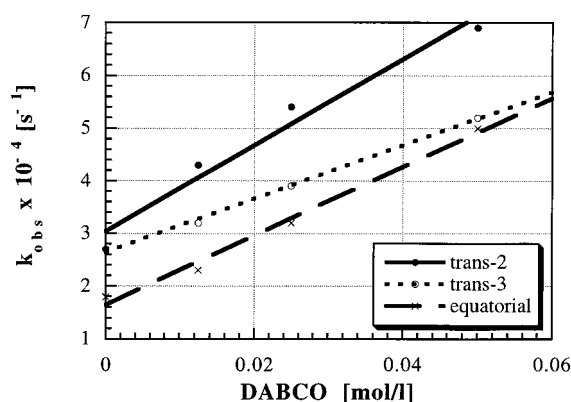
Figure 6. Plot of $k_{obs} = \ln 2/\tau_{1/2}$ vs [DABCO] for the reductive quenching of *e*-C$_{60}$[C(COO$^-$)$_2$]$_2$ (**2**) (×), *trans-3*-C$_{60}$[C(COO$^-$)$_2$]$_2$ (**3**) (○), and *trans-2*-C$_{60}$[C(COO$^-$)$_2$]$_2$ (**4**) (●) measured at 690, 670, and 670 nm, respectively.
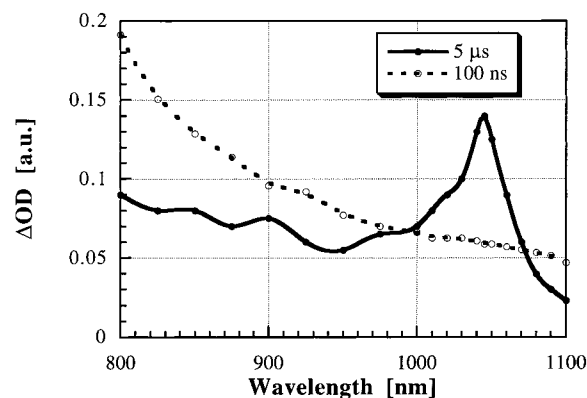

Figure 7. Differential absorption spectra obtained 100 ns (○) and 5 μs (●) upon flash photolysis at 337 nm of a nitrogen-saturated aqueous *e*-C$_{60}$[C(COO$^-$)$_2$]$_2$ (2.0×10^{-5} M) solution containing 0.05 M DABCO.

applied quencher concentration with the observed decay rate (see Figure 6). This suggests that the underlying process is due to a reductive quenching of *e*-($^3C_{60}$)[C(COO$^-$)$_2$]$_2$, probably involving an electron transfer from the electron-donating DABCO moiety to the excited triplet state of the functionalized fullerene. The intermolecular quenching rate constant of 7.2×10^5 M^{-1} s^{-1}, derived from the concentration dependence, reflects a significant slowdown relative to the water-soluble surfactant complex of pristine C$_{60}$, namely (C$_{60}$)$_{surfactant}$ (1.6×10^8 M^{-1} s^{-1}).[23] Furthermore, this trend indicates a substantial shift in the redox potential of the triplet excited state between the mono adduct and the equatorial bis adduct. The overall change of nearly 3 orders of magnitude, however, resembles the difference found for DABCO-induced quenching of the analogous ester derivatives, e.g., ($^3C_{60}$)C(COOEt)$_2$ and *e*-($^3C_{60}$)[C(COOEt)$_2$]$_2$, in nonpolar toluene.[19]

The above assumption of a reductive electron transfer implies formation of the respective fullerene π-radical anion, i.e., *e*-($C_{60}^{\bullet-}$)[C(COO$^-$)$_2$]$_2$. Figure 7 displays the differential absorption spectra monitored 100 ns and 5 μs after a 10 ns laser pulse at 337 nm of an aqueous *e*-C$_{60}$[C(COO$^-$)$_2$]$_2$ solution containing 0.05 M DABCO. The spectrum at the early time scale (100 ns) represents the near-IR tail of the *T_1→ *T_N absorption, which maximizes strongly at 690 nm. In contrast, the later spectrum unquestionably shows a characteristic near-IR absorption band with λ_{max} at 1055 nm. The comparability of this band with the diagnostic peak of various fullerene π-radical anions points to the formation of a charge-separated radical pair, e.g., {*e*-($C_{60}^{\bullet-}$) [C(COO$^-$)$_2$]$_2$/DABCO$^{\bullet+}$}, evolving from photoinduced electron

Bimolecular Electron and Energy Transfer Processes

J. Phys. Chem. B, Vol. 103, No. 9, 1999 **1449**

transfer and subsequent diffusional dissociation of the contact pair (eq 9). Further evidence for this postulate emerges from radical-induced reduction of this water-soluble fullerene derivative (see next section), yielding an absorption spectrum which resembles exactly the one monitored upon photolysis.

$$e\text{-}(^3C_{60})[C(COO^-)_2]_2 + DABCO \rightarrow$$
$$\{e\text{-}(C_{60}^{\bullet-})[C(COO^-)_2]_2 \cdots DABCO^{\bullet+}\} \rightarrow$$
$$e\text{-}(C_{60}^{\bullet-})[C(COO^-)_2]_2 + DABCO^{\bullet+} \quad (9)$$
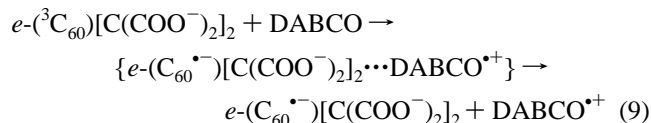
The 1055 nm absorption is relatively stable and decays slowly, over a few hundred microseconds, via quantitative recovery of the singlet ground state. The lifetime of the $e\text{-}(C_{60}^{\bullet-})[C(COO^-)_2]_2$ suffered a remarkable reduction with increasing fullerene concentration, at which increasingly higher yields of charge-separated radicals are generated. In our present study, the fullerene concentration was varied over a wide range [$(0.5-2.0) \times 10^{-5}$ M] and the decay was, in fact, found to be a second-order reaction, presumably between $e\text{-}(C_{60}^{\bullet-})\text{-}[C(COO^-)_2]_2$ and $DABCO^{\bullet+}$. Further evidence for this proposed second-order dynamic behavior and, thus, in turn, for a charge recombination mechanism emerges from a dose dependence study. The lifetime of the charge-separated radical pair at low $e\text{-}C_{60}[C(COO^-)_2]_2$ concentration is, for instance, impacted by a change in the laser energy. For example, at a given concentration of 1.0×10^{-5} M $e\text{-}C_{60}[C(COO^-)_2]_2$ (**2**) a lifetime of 405 μs was observed. By contrast, at the same fullerene concentration, $\tau = 230$ μs was measured at double the laser intensity. In summary, the ability of water molecules to shield the individual components of the generated radical pair via strong dipole—dipole interactions has a key function and is undoubtedly beneficial to retard the back electron-transfer process.

Quenching experiments involving the triplet excited states of *trans-3*-$C_{60}[C(COO^-)_2]_2$ (**3**) and *trans-2*-$C_{60}[C(COO^-)_2]_2$ (**4**) yielded similar rate constants for the DABCO-induced reduction, namely, 5.1×10^5 M^{-1} s^{-1} and 8.3×10^5 M^{-1} s^{-1}, respectively. The spectral region between 900 and 1100 nm shows again the time-resolved growths of the π-radical anion absorptions with maxima at 995 and 880 nm, for **3** and **4**, respectively, which match the accelerated decay of the triplet excited-state absorption.

Time-Resolved Radiolysis. *e-C_{60}[C(COO^-)_2]_2, trans-3-C_{60}[C(COO^-)_2]_2, trans-2-C_{60}[C(COO^-)_2]_2.* On the basis of the ground and excited-state properties, it seemed conceivable to carry out pulse radiolytic reductions of **2**−**5** without employing a hydrophilic host molecule, required for the water-soluble mono adduct (**1**). Indeed, upon radical-induced reduction of, for example, $e\text{-}C_{60}[C(COO^-)_2]_2$ (**2**) (5.0×10^{-6} M) in nitrogen-purged aqueous solution containing 10 vol % 2-propanol (pH 9.7), the kinetic traces showed an accelerated decay of the hydrated electrons transforming into a residual absorption. The UV/vis part of this residual absorption differs, however, from that reported for the reduction of pristine C_{60}. In particular, no bleaching occurs in the region around 330 nm. This deviation can be rationalized considering that the singlet ground-state spectrum of $e\text{-}C_{60}[C(COO^-)_2]_2$ lacks significant absorption bands in this range. However, the resolved fine structure of the transient product, comparable to ($C_{60}^{\bullet-}$), indicates a successful reduction of the fullerene core.

More importantly, the expected formation of the diagnostic near-IR transition band (see Figure 8) occurs synchronously with the decay of the electron absorption. In the present case, the fullerene π-radical anion, formed in the radiolysis, shows a
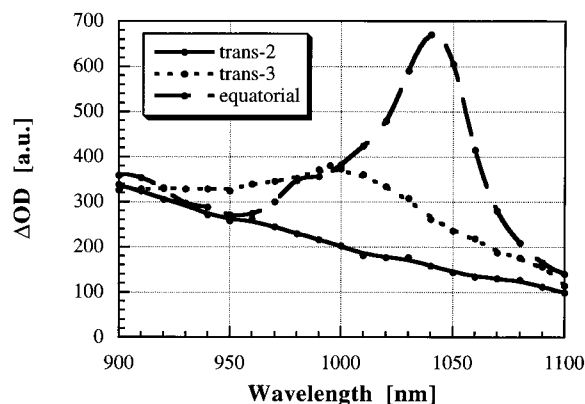

Figure 8. Differential absorption spectrum in the near-IR region of 10^{-5} M $e\text{-}C_{60}[C(COO^-)_2]_2$ (**2**) (●), *trans-3*-$C_{60}[C(COO^-)_2]_2$ (**3**) (×), and *trans-2*-$C_{60}[C(COO^-)_2]_2$ (**4**) (○) in nitrogen saturated aqueous solution containing 10 vol % 2-propanol (pH 9.7).
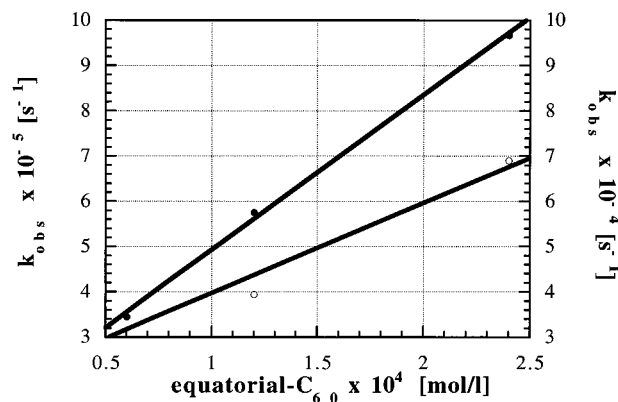
Figure 9. Plot of $k_{obs} = \ln 2/\tau_{1/2}$ vs [$e\text{-}C_{60}[C(COO^-)_2]_2$ (**2**)] for the reaction of e_{aq}^- (●) and $(CH_3)_2$•COH radicals (○) in aqueous solution containing 10 vol % 2-propanol (pH 9.7), respectively at 1055 nm.

pronounced absorption maximum at 1055 nm. Although the latter is somewhat blue-shifted relative to the analogous ester derivative, the current finding suggests that the underlying reaction is, indeed, the formation of $e\text{-}(C_{60}^{\bullet-})[C(COO^-)_2]_2$, initiated by hydrated electrons,

$$e\text{-}C_{60}[C(COO^-)_2]_2 + e_{aq}^- \rightarrow e\text{-}(C_{60}^{\bullet-})[C(COO^-)_2]_2 \quad (10)$$
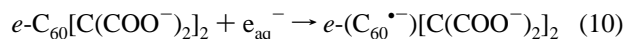
Upon increasing the fullerene concentration (($0.3-2.0) \times 10^{-5}$ M) an accelerated formation of the fullerene π-radical anion (monitored at 1055 nm) and decay of the hydrated electron absorption (at 700 nm) were found. The respective first-order rate constant versus concentration dependencies are linear (for illustration see Figure 9) and in good agreement with each other (Table 2), giving a bimolecular rate constant of 2.9×10^9 M^{-1} s^{-1} for the electron-induced reduction of $e\text{-}C_{60}[C(COO^-)_2]_2$. Analysis of the $e\text{-}(C_{60}^{\bullet-})[C(COO^-)_2]_2$ build-up kinetics throughout the UV−vis region confirmed this value. This value is, however, significantly lower than those published for the reduction of $(C_{60})_{surfactant}$, $(C_{60}C(COO^-)_2)_{surfactant}$, and the respective γ-CD encapsulated complexes (Table 3). Such an effect reflects the perturbation of the fullerene π-system by placing two negatively charged functional appendices onto the fullerene core.

It is interesting to note that the near-IR maximum of $e\text{-}(C_{60}^{\bullet-})\text{-}[C(COO^-)_2]_2$ (1040 nm) nearly coincides with that of pristine C_{60} (1080 nm). At first glance, this is a surprising observation, since the π-radical anion of the mono adduct, $(C_{60}^{\bullet-})C(COO^-)_2$ (1015 nm), displays a relatively strong blue shift which has been

TABLE 2: Rate Constant for the Radiation-Induced Reduction of Various Bisfunctionalized Fullerene Derivates in Homogeneous (H₂O, 10 vol % 2-Propanol, pH 9.7) and Heterogeneous (5% Triton X-100, 10 vol % 2-Propanol, pH 9.7) Aqueous Solutions
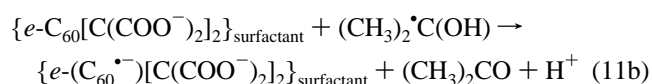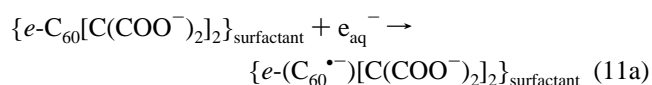
COMPOUND	MEDIUM	REAGENT	RATE CONSTANT $[10^{10} \text{ M}^{-1} \text{ S}^{-1}]$	PRODUCT; MAXIMUM [nm]
$e\text{-}C_{60}[C(COO^-)_2]_2$ **(2)**	H_2O	e_{aq}^-	0.29	$(C_{60}^{\bullet-})R; 1040$
	H_2O	$(CH_3)_3\overset{\bullet}{C}OH$	0.022	$(C_{60}^{\bullet-})R; 1040$
	H_2O/Triton	e_{aq}^-	0.34	$(C_{60}^{\bullet-})R; 1040$
	H_2O/Triton	$(CH_3)_3\overset{\bullet}{C}OH$	0.021	$(C_{60}^{\bullet-})R; 1040$
$trans\text{-}3\text{-}C_{60}[C(COO^-)_2]_2$ **(3)**	H_2O	e_{aq}^-	0.19	$(C_{60}^{\bullet-})R; 995$
	H_2O	$(CH_3)_3\overset{\bullet}{C}OH$	0.011	$(C_{60}^{\bullet-})R; 995$
	H_2O/Triton	e_{aq}^-	0.26	$(C_{60}^{\bullet-})R; 995$
	H_2O/Triton	$(CH_3)_3\overset{\bullet}{C}OH$	0.024	$(C_{60}^{\bullet-})R; 995$
$trans\text{-}2\text{-}C_{60}[C(COO^-)_2]_2$ **(4)**	H_2O	e_{aq}^-	0.34	$(C_{60}^{\bullet-})R; 880$
	H_2O	$(CH_3)_3\overset{\bullet}{C}OH$	0.019	$(C_{60}^{\bullet-})R; 880$
	H_2O/Triton	e_{aq}^-	0.32	$(C_{60}^{\bullet-})R; 880$
	H_2O/Triton	$(CH_3)_3\overset{\bullet}{C}OH$	0.02	$(C_{60}^{\bullet-})R; 880$
$e,e,e\text{-}C_{60}[C(COO^-)_2]_3$ **(5)**	H_2O	e_{aq}^-	0.075	$(C_{60}^{\bullet-})R; 1020$
	H_2O	$(CH_3)_3\overset{\bullet}{C}OH$	0.009	$(C_{60}^{\bullet-})R; 1020$

ascribed to the perturbation of the π-system, induced by the functionalization of the fullerene core. The near-IR maxima of the two radical anions from the trans adducts, namely, *trans-3*-$C_{60}[C(COO^-)_2]_2$ **(3)** and *trans-2*-$C_{60}[C(COO^-)_2]_2$ **(4)**, also differ significantly, with maxima at 995 and 880 nm, respectively. In conclusion, we notice a significant impact of the functionalization pattern on the optical properties.

Generally, clustering of fullerenes and functionalized fullerene derivatives can be avoided by embedding individual fullerene molecules into the hydrophobic interior of surfactant micelles, such as Triton X-100. Rate constants for truly monomer surfactant complexes have been determined, for example, for the reactions of hydrated electrons with pristine C_{60} (2.6×10^{10} $M^{-1} s^{-1}$), $C_{60}C(COO^-)_2$ **(2)** (1.7×10^{10} $M^{-1} s^{-1}$), and C_{60}-$(C_4H_{10}N^+)$ (3.5×10^{10} $M^{-1} s^{-1}$).[23]

Along this line, it seemed important to study the surfactant systems of **2**−**4** and to compare the associated spectral and kinetic data with those of the water-soluble monomer systems. Several important results emerged from these studies. First, the ground-state absorptions of surfactant solutions **2**−**4** are virtually superimposable with those recorded for aqueous fullerene solutions without a surfactant host. Furthermore, pulse radiolysis in deoxygenated aqueous solution resulted in differential spectra with near-IR absorptions at 1040, 995, and 880 nm for **2**, **3**,
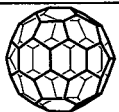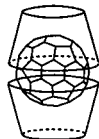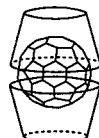
and **4**, respectively. Based on the similarity of these features with those noticed for the homogeneous systems, the observed spectra prove that the fullerene cores are reduced to their π-radical anions in these surfactant systems.

$$\{e\text{-}C_{60}[C(COO^-)_2]_2\}_{\text{surfactant}} + e_{aq}^- \rightarrow$$
$$\{e\text{-}(C_{60}^{\bullet-})[C(COO^-)_2]_2\}_{\text{surfactant}} \quad (11a)$$

$$\{e\text{-}C_{60}[C(COO^-)_2]_2\}_{\text{surfactant}} + (CH_3)_2\overset{\bullet}{C}(OH) \rightarrow$$
$$\{e\text{-}(C_{60}^{\bullet-})[C(COO^-)_2]_2\}_{\text{surfactant}} + (CH_3)_2CO + H^+ \quad (11b)$$

It is important to note that the spectral features of the surfactant-incorporated fullerenes are absolutely identical under comparable experimental conditions, which clearly points to a monomeric dissolution of the investigated fullerene derivatives in both systems, homogeneous and heterogeneous. This assumption is further corroborated by a comparison of the corresponding rate constants for the reduction of, for example, $\{e\text{-}C_{60}[C(COO^-)_2]_2\}_{\text{surfactant}}$ by hydrated electrons and $(CH_3)_2\overset{\bullet}{C}$-$(OH)$ radicals, which are to 3.4×10^9 $M^{-1} s^{-1}$ and 2.1×10^8 $M^{-1} s^{-1}$, respectively. In both cases, the similarity of the rates with the homogeneous systems are plausibly rationalized in terms of a successful suppression of the fullerene agglomeration.

Bimolecular Electron and Energy Transfer Processes

J. Phys. Chem. B, Vol. 103, No. 9, 1999 **1451**

TABLE 3: Rate Constant for the Radiation-Induced Reduction of Pristine C_{60} and Monofunctionalized Fullerene Derivatives in Homogeneous (H_2O, 10 vol % 2-Propanol) and Heterogeneous (5% Triton X-100, 10 vol % 2-Propanol) Aqueous Solutions[23,36]
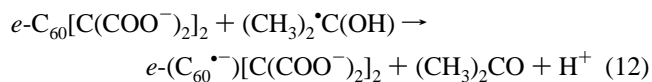
COMPOUND	MEDIUM	REAGENT	RATE CONSTANT $[10^{10}\ M^{-1}\ S^{-1}]$	PRODUCT; MAXIMUM [nm]
C_{60}	H_2O/Triton	e_{aq}^-	2.6	$C_{60}^{\bullet-}$; 1075
C_{60}	H_2O/Triton	$(CH_3)_3\overset{\bullet}{C}OH$	0.061	$C_{60}^{\bullet-}$; 1075
C_{60}/γ-CD	H_2O	e_{aq}^-	1.8	$C_{60}^{\bullet-}$; 1080
C_{60}/γ-CD	H_2O	$(CH_3)_3\overset{\bullet}{C}OH$	0.027	$C_{60}^{\bullet-}$; 1080
$C_{60}C(COO^-)_2$ (1)	H_2O/Triton	e_{aq}^-	1.7	$(C_{60}^{\bullet-})R$; 1015
$C_{60}C(COO^-)_2$ (1)	H_2O/Triton	$(CH_3)_3\overset{\bullet}{C}OH$	0.054	$(C_{60}^{\bullet-})R$; 1015
$C_{60}C(COO^-)_2/\gamma$-CD (1)	H_2O	e_{aq}^-	0.98	$(C_{60}^{\bullet-})R$; 1040
$C_{60}C(COO^-)_2/\gamma$-CD (1)	H_2O	$(CH_3)_3\overset{\bullet}{C}OH$	0.036	$(C_{60}^{\bullet-})R$; 1040

A comparison of the HOMO's and LUMO's of the mono adduct **1** with those of pristine C_{60} and the bis adducts **2**−**4** provides some further insight.[32] The molecular orbitals of **1** show a significant electron deficit in the singlet ground state, especially in the equatorial area. Reduction, by means of a one-electron addition into an accepting LUMO, has been proposed to lead to an electron distribution with a notable localization in the equatorial area. This may serve as supportive evidence to explain the substantial optical differences between ground-state, reduced-state, and excited-state spectra of pristine C_{60} and monofunctionalized fullerene derivatives. Selective introduction of a second functionalizing addend, especially into the equatorial area, has two major consequences. On one hand, it reintensifies the electron distribution of the singlet ground state in closer proximity to the equatorial position and, second, it homogenizes the corresponding LUMO level, resembling the one known for pristine C_{60}. It is interesting to note that this effect reaches its maximum for the e-$C_{60}[C(COO^-)_2]_2$ adduct. This emerges from the analysis of the corresponding electron distributions in the LUMO's of the trans-*3* and trans-*4* adducts. Unmistakably, these imply a strong perturbation of the π-electron density, comparable to that shown for the mono adduct **1**.

Cyclic voltammetric investigations show a correlation between the stepwise transformation of sp^2-hybridized carbons into sp^3-hybridized analogues and a significant shift of the associated redox potential.[33−35] Generally, both the reduction and oxidation potentials, are progressively shifted to more negative values. Furthermore, we believe that the presence of negatively charged carboxyl groups on the fullerene periphery also contributes to the overall slower rate constants by impacting the reaction with the negatively charged electrons through Coulomb repulsion.

Applying a less powerful, but more selective reductant, e.g., the $(CH_3)_2\overset{\bullet}{C}(OH)$ radical, sheds further supporting light onto this issue. Pulse radiolysis of **2**, under conditions outlined in eqs 2 and 4, showed the diagnostic NIR absorption at 1055 nm, confirming the fullerene reduction via

$$e\text{-}C_{60}[C(COO^-)_2]_2 + (CH_3)_2\overset{\bullet}{C}(OH) \rightarrow$$
$$e\text{-}(C_{60}^{\bullet-})[C(COO^-)_2]_2 + (CH_3)_2CO + H^+ \quad (12)$$

As expected, the observed rate ($k_{obs} = \ln 2/\tau_{1/2}$) was found to be linearly dependent on the fullerene concentration. The rate constant is $2.2 \times 10^8\ M^{-1}\ s^{-1}$, slightly slower than the $(CH_3)_2\overset{\bullet}{C}$-(OH) radical-induced reduction of the C_{60}/γ-CD and $C_{60}C$-$(COO^-)_2/\gamma$-CD complexes.

Pulse radiolytic reduction studies of trans-*3*-$C_{60}[C(COO^-)_2]_2$ (**3**) and trans-*2*-$C_{60}[C(COO-)_2]_2$ (**4**) at pH 9.7 led to overall similar observations. In particular, π-radical anion absorptions were noticed at 995 and 880 nm, for **3** and **4**, respectively. Likewise, the rate constants for the two trans adducts, $1.1 \times 10^8\ M^{-1}\ s^{-1}$ (trans-*3*-$C_{60}[C(COO^-)_2]_2$,(**3**)) and $1.9 \times 10^8\ M^{-1}$ s^{-1} (trans-*2*-$C_{60}[C(COO^-)_2]_2$ (**4**)), are only insignificantly affected relative to the equatorial isomer (**2**).

e,e,e-$C_{60}[C(COO^-)_2]_3$. Although pulse radiolytic reduction of 1.0×10^{-5} M e,e,e-$C_{60}[C(COO^-)_2]_3$ (**5**) in aqueous solution (10 vol % 2-propanol, pH 9.7) does not show any bleaching around the fullerene's 330 nm band, the transient differential spectrum displays ground-state bleaching of the 276 nm band. Furthermore, the UV−vis region is dominated by a pronounced fine structure. Regarding the diagnostic near-IR band, e,e,e-$(C_{60}^{\bullet-})[C(COO^-)_2]_3$ is characterized by an absorption maximum at 1020 nm. This value is slightly shifted relative to the π-radical anion absorption of the analogous ester derivative, e,e,e-$(C_{60}^{\bullet-})$-$[C(COOEt)_2]_3$, in nonpolar organic solvents. Addition of various concentrations of **5** in the range of $(2.5−11) \times 10^{-5}$ M resulted
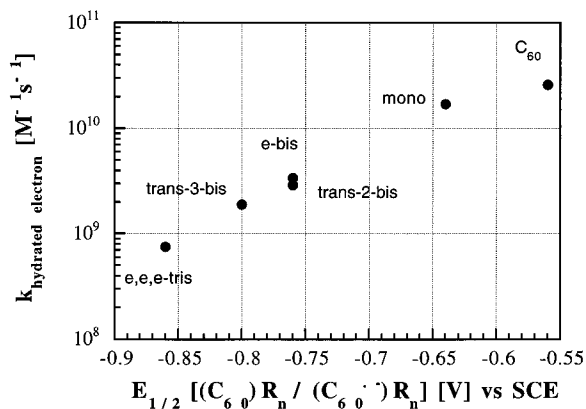
Figure 10. Semilogarithmic plot of $k(e_{aq}^-)$ vs redox potential for the first reduction step of C_{60} and functionalized fullerene derivatives (**1**–**5**) in 1,2-dichloroethane solutions.

in an accelerated decay of the electron absorption at 700 nm. To verify the associated kinetics, we monitored likewise at 1020 nm and various wavelengths in the 970–1100 nm range and we derived a rate constant of $7.5 \times 10^8 \text{ M}^{-1} \text{ s}^{-1}$ from the decay at 700 nm and $6.7 \times 10^8 \text{ M}^{-1} \text{ s}^{-1}$ from the growing-in at 1020 nm. These two values are in reasonable agreement, considering the relatively large error margins which need to be allowed for kinetic measurements from the relatively weak IR signals. They show that the reduction of the fullerene core in **5** is slower relative to the less functionalized mono and bis adducts.

Relation Between Reduction Potential and Reduction Rate Constants. The accessibility of water-soluble fullerene derivatives and the acquisition of their physicochemical properties for the first time allows establishment of a thermodynamic relationship for pristine C_{60}, mono adduct **1**, bis adducts **2**–**4**, and tris adduct **5**. In an earlier study, we reported that multiple functionalization of the fullerene core shows a substantial impact on the reduction potential, as evaluated from cyclic voltamograms in toluene/2-propanol (9:1).[20] However, this solvent mixture resulted in a decline of reversibility for the underlying reduction processes. Therefore, we measured the redox potential for the first reduction step of the various compounds in a solvent that (i) allows the functionalized fullerene derivatives to dissolve at high concentrations, (ii) is commonly applied in cyclic voltametric studies, and (iii) sustains the reversibility of the electron transfer, namely, 1,2 dichloroethane (1,2 DCE). The respective values are listed in Table 1. It is interesting to note that even in this solvent the tris adduct **5**, in contrast to all others, still displays a complete irreversible reduction step.

A semilogarithmic correlation of these newly measured redox potentials versus the rate constants for the reduction, induced by the hydrated electron, is plotted in Figure 10. The linear dependence demonstrates that decreasing the driving force for electron transfer, i.e., the difference in reduction potential between the hydrated electron and the first reduction step of the fullerene, results, in turn, in a substantial slow-down of the rate constant.

Conclusion

Steady-state and time-resolved measurements with a series of bis-functionalized fullerene derivatives (**2**–**4**) and a single tris-functionalized adduct (**5**) provide evidence that they are monomeric in aqueous media. An earlier observation regarding their water-insoluble precursors, namely, malonic acid diethyl ester derivatives, demonstrated that functionalization of C_{60} leads to a perturbation of the fullerenes π-systems, the degree of

which, relative to pristine C_{60}, has been shown to intensify with increasing number of functionalizing addends. The overall impact is mainly governed by electronic factors. This clearly also applies for the hydrolyzed and water soluble derivatives **2**–**5**, as shown by a deceleration of the reduction processes in the singlet ground and triplet excited state, and comparable blue shifts of the respective absorption bands in the near-IR.

Besides the perturbation of the π-system, polyderivatization reduces the number of reactive sites on the fullerene surface due to sp^3 carbon hybridization and eventually leads to fullerene derivatives that show less and less resemblance to the original C_{60}. Considering the fullerene reactivity, any of the bis adducts clearly outperform the e,e,e-$C_{60}[C(COO^-)_2]_3$ (**5**) derivative, while the γ-CD-encapsulated complexes of C_{60} and $C_{60}C(COO^-)_2$ (**1**) are, despite their heterogeneous nature, still better electron acceptor units than the bis adducts.

We are currently probing bis-functionalized pyrrolidinium derivatives as electron acceptors to further unravel the effect of electrostatic repulsion or attraction forces between the fullerene derivatives and reducing radicals.

References and Notes

(1) Haddon, R. C. *Acc. Chem. Res.* **1988**, *21*, 243–249.
(2) Mauser, H.; Hommes, N. J. R. v. E.; Clark, T.; Hirsch, A.; Pietzak, B.; Weidinger, A.; Dunsch, L. *Angew. Chem., Int. Ed. Engl.* **1997**, *36*, 2835–2838.
(3) Haddon, R. C.; Brus, L. E.; Raghavachari, K. *Chem. Phys. Lett.* **1986**, *131*, 165.
(4) Haddon, R. C.; Brus, L. E.; Raghavachari, K. *Chem. Phys. Lett.* **1986**, *125*, 459.
(5) Dubois, D.; Kadish, K. M.; Flanagan, S.; Wilson, L. J. *J. Am. Chem. Soc.* **1991**, *113*, 7773–7774.
(6) Dubois, D.; Kadish, K. M.; Flanagan, S.; Haufler, R. E.; Chibante, L. P. F.; Wilson, L. J. *J. Am. Chem. Soc.* **1991**, *113*, 4364–4366.
(7) Jehoulet, C.; Bard, A. J.; Wudl, F. *J. Am. Chem. Soc.* **1991**, *113*, 5456–5457.
(8) Imahori, H.; Hagiwara, K.; Akiyama, T.; Aoki, M.; Taniguchi, S.; Okada, T.; Shirakawa, M.; Sakata, Y. *Chem. Phys. Lett.* **1996**, *263*, 545–550.
(9) Guldi, D. M.; Asmus, K.-D. *J. Am. Chem. Soc.* **1997**, *119*, 5744–5745.
(10) Imahori, H.; Sakata, Y. *Adv. Mater.* **1997**, *9*, 537–546.
(11) Jensen, A. W.; Wilson, S. R.; Schuster, D. I. *Bioorg. Med. Chem.* **1996**, *4*, 767–779.
(12) Diederich, F.; Thilgen, C. *Science* **1996**, *271*, 317–323.
(13) Hirsch, A. *The Chemsitry of the Fullerenes*; Georg Thieme Verlag: Stuttgart, 1994.
(14) Prato, M. *J. Mater. Chem.* **1997**, *7*, 1097–1109.
(15) Prato, M.; Maggini, M. *Acc. Chem. Res.* **1998**, *31*, 519–526.
(16) Bingel, C. *Chem. Ber.* **1993**, *126*, 1957–1959.
(17) Lamparth, I.; Maichle-Mössmer, C.; Hirsch, A. *Angew. Chem., Int. Ed. Engl.* **1995**, *34*, 1607–1609.
(18) Lamparth, I.; Hirsch, A. *J. Chem. Soc., Chem. Commun.* **1994**, 1727–1728.
(19) Guldi, D. M.; Hungerbühler, H.; Asmus, K.-D. *J. Phys. Chem.* **1995**, *99*, 9380–9385.
(20) Guldi, D. M.; Asmus, K.-D. *J. Phys. Chem. A* **1997**, *101*, 1472–1481.
(21) Guldi, D. M.; Hungerbühler, H.; Asmus, K.-D. *J. Phys. Chem. A* **1997**, *101*, 1783.
(22) Guldi, D. M.; Hungerbühler, H.; Asmus, K.-D. *J. Phys. Chem.* **1995**, *99*, 13487–13493.
(23) Guldi, D. M. *J. Phys. Chem. A* **1997**, *101*, 3895–3900.
(24) Guldi, D. M.; Liu, D.; Kamat, P. V. *J. Phys. Chem. A* **1997**, *101*, 6195–6201.
(25) Hug, G. L.; Wang, Y.; Schöneich, C.; Jiang, P. Y.; Fessenden, R. W. *Radiat. Phys. Chem.*, submitted.
(26) Ebbesen, T. W. *Rev. Sci. Instrum.* **1988**, *59*, 1307–1309.
(27) Thomas, M. D.; Hug, G. L. *Comput. Chem.* **1998**, *22*, 491–498.

(28) Foote, C. S. *Top. Curr. Chem.* **1994**, *169*, 348−363.

(29) Arbogast, J. W.; Darmanyan, A. P.; Foote, C. S.; Rubin, Y.; Diederich, F. N.; Alvarez, M. M.; Anz, S. J.; Whetten, R. L. *J. Phys. Chem.* **1991**, *95*, 11−12.

(30) Arbogast, J. W.; Foote, C. S. *J. Am. Chem. Soc.* **1991**, *113*, 8886−8889.

(31) Murov, S. L.; Carmichael, I.; Hug, G. L. *Handbook of Photochemistry*; Marcel Dekker: New York, 1993.

(32) Hirsch, A.; Lamparth, I.; Schick, G. *Liebigs. Ann.* **1996**, 1725−1734.

(33) Arias, F.; Echegoyen, L.; Wilson, S. R.; Lu, Q.; Lu, Q. *J. Am. Chem. Soc.* **1995**, *117*, 1422−1427.

(34) Boudon, C.; Gisselbrecht, J.-P.; Gross, M.; Isaacs, L.; Anderson, H. L.; Faust, R.; Diederich, F. *Helv. Chim. Acta* **1995**, *78*, 1334−1344.

(35) Kessinger, R.; Gomez-Lopez, M.; Boudon, C.; Gisselbrecht, J.-P.; Gross, M.; Echegoyen, L.; Diederich, F. *J. Am. Chem. Soc.* **1998**, *120*, 8545−8546.

(36) Priyadarsini, K. I.; Mohan, H.; Mittal, J. P.; Guldi, D. M.; Asmus, K.-D. *J. Phys. Chem.* **1994**, *98*, 9565−9569.